



# A Geometrically Non-linear Stochastic Analysis of Two-dimensional Structures made of Neo-hookean Hyperelastic Materials Using MLPG Method: Considering Uncertainty in Mechanical Properties

M. H. Ghadiri Rad<sup>1\*</sup>, F. Shahabian<sup>2</sup>, S. M. Hosseini<sup>3</sup>

<sup>1</sup> Engineering Department, Quchan University of Technology, Quchan, Iran

<sup>2</sup> Civil Engineering Department, Faculty of Engineering, Ferdowsi University of Mashhad, Mashhad, Iran

<sup>3</sup> Industrial Engineering Department, Faculty of Engineering, Ferdowsi University of Mashhad, Mashhad, Iran

**ABSTRACT:** In recent decades, analysis of structures considering variability of some parameters for more reliable design has attracted the attention of researchers. In this paper, the stochastic analysis of a cantilever deep beam made of large deformable neo-hookean material is carried out. For this purpose, the meshless local Petrov-Galerkin (MLPG) method is developed to obtain the geometrically non-linear equilibrium equations. The radial point interpolation method is used for generating the shape functions. The incremental iterative Newton-Raphson method with suitable load steps is used to solve the non-linear governing equations. The results of deterministic analysis obtained with proposed method are compared with the finite element results and good agreement is achieved. The initial elasticity modulus of neo-hookean material is considered to be uncertain variable. To generate random field of uncertain variable with normal, lognormal and uniform probability density functions (PDFs), the Monte Carlo Simulation (MCS) technique was employed. The sufficient number of simulations for convergence the results was determined experimentally. The effect of elasticity modulus, PDF and coefficients of variation (COV) on maximum vertical displacement, PDF and COV of results are studied in details. Comparing the stochastic and deterministic results shows that the uncertainty in mechanical properties has significant effect on results.

## Review History:

Received: 30 May 2018

Revised: 19 August 2018

Accepted: 31 August 2018

Available Online: 11 September 2018

## Keywords:

Stochastic Analysis

Large Deformation

Hyperelastic Material

Monte-Carlo Simulation

Meshless Local Petrov-Galerkin Method

## 1- Introduction

Structural analysis generally is faced with some uncertainties in related parameters such as applied loads, material properties, geometry and other quantities. Analysis of structures considering variability of parameters yields to more reliable design. Hence, stochastic analysis has found extensive attention by researchers in recent decades. Chakraborty and Bhattacharyya proposed a stochastic finite element method for determining response variability for three-dimensional (3D) static problems subjected to spatial uncertainties of the material properties [1]. In their work the random parameters were generated using the Monte-Carlo Simulation (MCS) technique. Xu et al. investigated free vibration of functionally graded (FG) beam in which both physical parameters of each constituent material and material distribution are treated as random variables with low variability [2]. Singh et al. examined the influence of random variables on the free vibration of shear deformable composite plates using the finite element method in conjunction with first order perturbation

technique [3]. Sakata et al. employed the perturbation method and the finite difference method, analyzed a stochastic homogenization problem of a periodic porous material considering a microscopic geometrical random variation [4]. Naskar et al. developed the stochastic representative volume element (SRVE) to quantify the probabilistic variability in free vibration responses of damaged thin-walled laminated composite beams due to spatially random stochasticity in the micro-mechanical and geometric properties [5]. Onkar et al. proposed a stochastic finite element formulation for the buckling analysis of laminated plates with random material properties using perturbation technique [6]. A comparison among three methodologies usually employed in stochastic analysis of structures including direct Monte-Carlo method, perturbation techniques and theory of fuzzy sets presented by Lima and Ebecken [7].

Some researches in the stochastic and reliability field of structures have been carried out using the meshless method that do not require a structured mesh to discretize the problem domain. Hosseini and Shahabian using the MCS studied on the effect of variation in material properties on dynamic response of FG thick hollow cylinders under mechanical shock loading

Corresponding author, E-mail: hosein\_ghadiri@qiet.ac.ir

[8, 9]. Rao and Rahman developed the enriched element-free Galerkin method for analysis of elastic-plastic cracked structures with uncertainties in load, material properties, and crack geometry [10]. They used the first-order reliability method (FORM) for predicting probabilistic fracture response and reliability of cracked structures. The propagation of thermal and elastic waves in the FG thick hollow cylinder with uncertainty in mechanical properties using the MLPG method under thermal shock loading is studied by Hosseini et al. [11]. The application of meshless method for solving stochastic advection-diffusion equations based on radial basis functions was developed by Dehghan and Shirzadi [12]. Su et al. presented the stochastic spline fictitious boundary element method for modal analysis of plane elastic problems in which the structural parameters modeled as random fields [13].

Hyperelastics are special case of large deformable materials in which the stress-strain relationship derives from a strain energy density function. Neo-hookean, Mooney-Rivlin and Ogden are three hyperelastic material models which are widely used in articles [14]. Anani and Rahimi studied on thick walled spherical shells composed of functionally graded incompressible neo-hookean hyperelastic materials [15]. Soares and Gonçalves investigated large-amplitude vibrations of a rectangular hyperelastic membrane [16]. In their work, geometric non-linearity due to finite deformations was taken in to account and material non-linearity were described by deformations of a hyperelastic body described by Ogden’s model under impact loading is done by Feng et al. [17].

Despite the finite element method (FEM) is a standard analytical tool for the large deformation problems, extremely large deformations and the nearly incompressible nature of hyperelastic materials, cause to some drawbacks such as mesh distortion in applying this method. Since no mesh is used in meshless method, it is an effective method for large deformation problems. In this method, distorted geometry doesn’t have a negative impact on the solution accuracy [18]. Gu et al. developed a meshless method based on the total Lagrangian (TL) approach for large deformation problems [19]. They computed the material moduli using the strain energy density function given for hyperelastic compressible neo-hookean materials. Ghadiri rad et al. proposed a MLPG method for elasto-dynamic analysis of geometrically non-linear two dimensional (2D) domains made of neo-hookean hyper-elastic functionally graded materials [20, 21].

In this paper, the stochastic analysis of hyperelastic materials with large deformation is carried out using the geometrically nonlinear MLPG method. The neo-hookean model is employed to model hyper elasticity of material. The initial elasticity Modulus of neo-hookean material is supposed to be uncertain where randomly generated using the MCS in which over 1000 samples are generated for each set of analytical results. The effect of elasticity modulus PDF and COV on maximum vertical displacement, PDF and COV of results are studied in details.

## 2- Stochastic hyperelastic constitutive model

In geometrically non-linear analysis of some materials, such as rubber like materials, linear elastic model is not consistent with the test data. The stress-strain behavior of such materials can be defined using hyperelastic models. In these models, the second Piola-Kirchhoff stresses, the stresses computed

with respect to the initial configuration, can be derived from a strain energy density function per unit of un-deformed volume which is denoted by ‘W’. The compressible neo-hookean model is a hyperelastic material model in which the strain energy density function is expressed as follow:

$$W = \frac{\mu_0}{2}(I_1 - 3) - \mu_0 \ln J + \frac{\lambda_0}{2}(\ln J)^2 \quad (1)$$

Where ‘ $\mu_0$ ’ and ‘ $\lambda_0$ ’ are the Lamé constants at the initial configuration. ‘ $I_1$ ’ is the first strain invariant and ‘J’ is determinant of deformation gradient tensor ‘F’. The initial elasticity modulus ‘E’ and Poisson ratio ‘ $\nu$ ’ are related to the Lamé constants using the following equations.

$$\mu_0 = \frac{E}{2(1+\nu)} \quad (2)$$

$$\lambda_0 = \frac{E}{2(1+\nu)(1-2\nu)} \quad (3)$$

The initial elasticity modulus is considered as uncertain property which is generated using the equations presented in Table 1. In this table, ‘z(i)’ is the standard normal random number at the ‘i’th simulation and The PDF stands for the probability density function which maps the standard random numbers on to the real values [22]. In the normal probability density function, the PDF of random variable ‘X’ are bell-shaped. The random variable is a lognormal if the ‘ $y=\ln(X)$ ’ is normally distributed. For a uniform random variable, the PDF has a constant value for all random variable located in the sample space. The most important PDFs used in reliability analysis of structures are introduced in details in Nowak and Collins’s book [22].

## 3- Deformation gradient tensor

In large deformation analysis, two different configuration can be imagined for a body: initial configuration and current configuration (see Figure 1). According to Figure 1, the following relation can be written between the position vectors in the initial and current configuration which are denoted by ‘ $X_i$ ’ and ‘ $x_i$ ’ respectively.

$$x_i = X_i + u_i \quad (4)$$

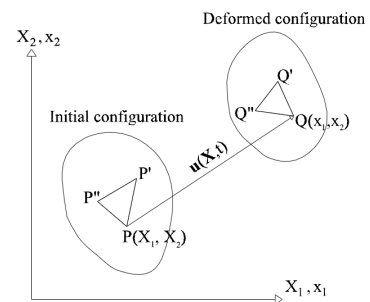


Figure 1. Initial and deformed configuration of a body with finite deformation

**Table 1. The equations for generating random elasticity modulus in various PDFs [22]**

PDF	Parameters	Expression
Normal	$\mu_E = \text{mean}(E)$ $\sigma_E = \text{variance}(E)$	$E(i) = \mu_E + \sigma_E z(i)$
Lognormal	$\sigma_{\ln E} = \sqrt{\ln\left(\left(\frac{\mu_E}{\sigma_E}\right)^2 + 1\right)}$ $\mu_{\ln E} = \ln(\mu_E) - 0.5(\sigma_{\ln E})^2$	$E(i) = \exp[\mu_{\ln E} + \sigma_{\ln E} z(i)]$
Uniform	$a = \mu_E - \sqrt{3}\sigma_E$ $b = \mu_E + \sqrt{3}\sigma_E$	$E(i) = a + (b - a)z(i)$

where 'u<sub>i</sub>' is the displacement vector. Using the chain rule, the relationship between 'dx<sub>i</sub>' and 'dX<sub>i</sub>' can be readily obtained as follows.

$$dx_i = \frac{\partial x_i}{\partial X_j} dX_j = F_{ij} dX_j \tag{5}$$

where 'F<sub>ij</sub>' is called deformation gradient tensor. Substituting Equation 4 into Equation 5 yields to:

$$F_{ij} = \frac{\partial X_i}{\partial X_j} + \frac{\partial u_i}{\partial X_j} = \delta_{ij} + \frac{\partial u_i}{\partial X_j} \tag{6}$$

'δ<sub>ij</sub>' is Kronecker delta function. The last equation can be rewritten in the following matrix notation:

$$[F] = \begin{bmatrix} F_{xx} & F_{xy} \\ F_{yx} & F_{yy} \end{bmatrix} = \begin{bmatrix} 1 + \frac{\partial u}{\partial X} & \frac{\partial u}{\partial Y} \\ \frac{\partial v}{\partial X} & 1 + \frac{\partial v}{\partial Y} \end{bmatrix} \tag{7}$$

Deformation gradient vector can be defined similar to the stress vectors.

$$\{F\} = \begin{Bmatrix} F_{xx} \\ F_{yy} \\ F_{xy} \\ F_{yx} \end{Bmatrix} = \begin{Bmatrix} 1 + \frac{\partial u}{\partial X} \\ 1 + \frac{\partial v}{\partial Y} \\ \frac{\partial u}{\partial Y} \\ \frac{\partial v}{\partial X} \end{Bmatrix} = \begin{Bmatrix} 1 \\ 1 \\ 0 \\ 0 \end{Bmatrix} + \begin{Bmatrix} \frac{\partial u}{\partial X} \\ \frac{\partial v}{\partial Y} \\ \frac{\partial u}{\partial Y} \\ \frac{\partial v}{\partial X} \end{Bmatrix} \tag{8}$$

Thus, the increment of deformation gradient vector can be obtained as:

$$\{\Delta F\} = \begin{bmatrix} \frac{\partial}{\partial X} & 0 \\ 0 & \frac{\partial}{\partial Y} \\ \frac{\partial}{\partial Y} & 0 \\ 0 & \frac{\partial}{\partial X} \end{bmatrix} \begin{Bmatrix} \Delta u \\ \Delta v \end{Bmatrix} \tag{9}$$

Using the shape function matrix '[N]' the displacement functions 'u' and 'v' can be expressed with respect to its nodal values at the 'n' nodes located in support domain.

$$\begin{Bmatrix} u \\ v \end{Bmatrix} = \sum_{i=1}^n \begin{bmatrix} N_i & 0 \\ 0 & N_i \end{bmatrix} \begin{Bmatrix} D_{2i-1} \\ D_{2i} \end{Bmatrix} \tag{10}$$

Substituting the last equation into Equation 9, yields the increment of deformation gradient vector with respect to the nodal displacement.

$$\{\Delta F\} = \sum_{i=1}^n \begin{bmatrix} \frac{\partial N_i}{\partial X} & 0 \\ 0 & \frac{\partial N_i}{\partial Y} \\ \frac{\partial N_i}{\partial Y} & 0 \\ 0 & \frac{\partial N_i}{\partial X} \end{bmatrix} \begin{Bmatrix} \Delta D_{2i-1} \\ \Delta D_{2i} \end{Bmatrix} \tag{11}$$

$$\{\Delta F\} = [B]\{\Delta D\} \tag{12}$$

where:

$$[B] = [B_1 \ B_2 \ \dots \ B_n] \tag{13}$$

$$[B_i] = \begin{bmatrix} \frac{\partial N_i}{\partial X} & 0 \\ 0 & \frac{\partial N_i}{\partial Y} \\ \frac{\partial N_i}{\partial Y} & 0 \\ 0 & \frac{\partial N_i}{\partial X} \end{bmatrix} \quad (14)$$

**4- MLPG formulation**

In large deformation theory, two configurations including initial and current configurations can be considered for a body (see Figure 1). It should be mentioned that the real forces and geometry of problem can be defined merely in the current configuration. The differential equilibrium equation of a hyperelastic body at the current configuration is described as:

$$\sigma_{ji,j} + b_i = 0 \quad (15)$$

where ‘ $b_i$ ’ is the body force and ‘ $\sigma_{ji}$ ’ is the Cauchy stress tensor. It should be mentioned that three stress tensors including Cauchy ‘ $\sigma_j$ ’, 1st Piola-Kirchhoff ‘P’ and second Piola-Kirchhoff ‘S’ can be defined in large deformation theory. The Cauchy and second Piola-Kirchhoff stress tensors give the stress state in the deformed and initial configurations, respectively. The 1<sup>st</sup> Piola-Kirchhoff stress tensor is called nominal stress tensor and defined as applied forces at the current configuration to the area in the reference configuration. Since before the analysis, the deformed configuration of body is unknown, the 1<sup>st</sup> Piola-Kirchhoff stress is useful to obtain the equilibrium equation at the undeformed configuration in total lagrangian approach. Thus, one can write the equilibrium equation with respect to the initial configuration as follow [23]:

$$P_{ji,j} + b_i = 0 \quad (16)$$

Using the weight function ‘ $W_i$ ’ in local subdomains at the initial configuration ‘ $\Omega$ ’, the weak-form of Equation 16 will be obtained.

$$\int_{\Omega} (P_{ji,j} + b_i) W_i d\Omega = 0 \quad (17)$$

The following relation between the 1st and second piola-Kirchhoff stress tensors can be easily derived.

$$P_{ij} = S_{ik} F_{jk} \quad (18)$$

Applying gauss divergence theorem to the Equation 17, using stress-strain and strain-displacement relationships and after performing some calculations, this equation can be converted the following incremental matrix form [23].

$$[K_T]\{\Delta D\} = \{\Delta P\} \quad (19)$$

where, ‘ $[K_T]$ ’ is the tangent stiffness matrix and ‘ $\{\Delta P\}$ ’ is the equivalent incremental nodal force vector which can be obtained from the following equations:

$$[K_T] = \int_{\Omega} [w']([\bar{F}][D_m][B^{nl}] + [\bar{S}][B]) d\Omega - \int_{\Gamma_i + \Gamma_o} [w][N]([\bar{F}][D_m][B^{nl}] + [\bar{S}][B]) d\Gamma \quad (20)$$

$$\{\Delta P\} = \int_{\Gamma_i} [w]\{\bar{T}\} d\Gamma - \int_{\Omega} [w'][\bar{F}]\{S\} d\Omega + \int_{\Gamma_i + \Gamma_o} [w][N][\bar{F}]\{S\} d\Gamma \quad (21)$$

In the recent equations, some matrices are used which are introduced in the following equations:

$$[W'] = \begin{bmatrix} w_{,x} & 0 & 0 & w_{,y} \\ 0 & w_{,y} & w_{,x} & 0 \end{bmatrix} \quad (22)$$

$$\{\bar{T}\} = \begin{Bmatrix} \bar{T}_x \\ \bar{T}_y \end{Bmatrix} = \begin{Bmatrix} \sigma_{xx} n_x + \sigma_{yx} n_y \\ \sigma_{xy} n_x + \sigma_{yy} n_y \end{Bmatrix} \quad (23)$$

$$[B^{nl}] = [B_1^{nl} \quad B_2^{nl} \quad \dots \quad B_n^{nl}] \quad (24)$$

$$[B_i^{nl}] = \begin{bmatrix} F_{xx} \frac{\partial N_i}{\partial X} & F_{yx} \frac{\partial N_i}{\partial X} \\ F_{xy} \frac{\partial N_i}{\partial Y} & F_{yy} \frac{\partial N_i}{\partial Y} \\ F_{xy} \frac{\partial N_i}{\partial X} + F_{xx} \frac{\partial N_i}{\partial Y} & F_{yx} \frac{\partial N_i}{\partial Y} + F_{yy} \frac{\partial N_i}{\partial X} \end{bmatrix} \quad (25)$$

$$[\bar{S}] = \begin{bmatrix} S_{xx} & 0 & S_{xy} & 0 \\ 0 & S_{yy} & 0 & S_{xy} \\ 0 & S_{xy} & 0 & S_{xx} \\ S_{xy} & 0 & S_{yy} & 0 \end{bmatrix}, [\bar{F}] = \begin{bmatrix} F_{xx} & 0 & F_{xy} \\ 0 & F_{yy} & F_{yx} \\ F_{yx} & 0 & F_{yy} \\ 0 & F_{xy} & F_{xx} \end{bmatrix} \quad (26)$$

‘ $N_i$ ’ In Equation 25, is the shape function at the node ‘i’. In this paper, the radial point interpolation method (RPIM) is employed to construct the shape function.

**5- RPIM shape function**

One of the well-established methods for geometrically non-linear analysis of structures is the finite element method. However, extremely large deformations and the nearly incompressible nature of hyper-elastic materials cause to some drawbacks such as mesh distortion in applying this method. The mesh regeneration process in spite of prevention excessive element distortion, increases the time of analysis.

In meshless methods the distributed nodes in problem domain, rather than the meshing, are used for discretization of problem domain and its boundaries. Because no mesh is used in these methods, extremely large deformations doesn't have a negative impact on the solution accuracy.

The displacement field function ‘u’ can be interpolated by function ‘ $u^h$ ’ which is in terms of nodal values of displacement at the all nodes located in support domain ‘ $\Omega_s$ ’ of point ‘ $x_Q$ ’, using the following equation:

$$u^h(\mathbf{x}) = \sum_{i=1}^n a_i R_i(\mathbf{x}) = [R]\{a\} \quad (27)$$

$$\mathbf{x} = \{x \quad y\}^T$$

where, ‘ $a_1, a_2, \dots, a_n$ ’ are unknown coefficients and ‘ $[R]$ ’ is the radial basis function (RBF) at the all nodes located in ‘ $\Omega_s$ ’.

Many types of RBFs are used in literature such as Gaussian, thin plate, splineradial and multi-quadric basis functions [24]. In this paper, multi-quadric basis function with the following expression is used.

$$R_i(\mathbf{x}) = \left( (x-x_i)^2 + (y-y_i)^2 + c^2 \right)^q \quad (28)$$

where, 'c' and 'q' are constant parameters which are experimentally determined as 'c=0.5' and 'q=1.03' to provide the best accuracy. The unknown coefficients 'a<sub>1</sub>, a<sub>2</sub>, ..., a<sub>n</sub>' can be calculated by applying the Equation 27 at the all nodes located in 'Ω<sub>s</sub>'.

$$\{D\} = [R_0] \{a\} \quad (29)$$

where, '{D}' is the nodal values of displacement field function and '[R<sub>0</sub>]' is the moment matrix which is contains the nodal values of matrix '[R]'.

$$[R_0] = \begin{bmatrix} R_1(\mathbf{x}_1) & R_2(\mathbf{x}_1) & \cdots & R_n(\mathbf{x}_1) \\ R_1(\mathbf{x}_2) & R_2(\mathbf{x}_2) & \cdots & R_n(\mathbf{x}_2) \\ \vdots & \vdots & \ddots & \vdots \\ R_1(\mathbf{x}_n) & R_2(\mathbf{x}_n) & \cdots & R_n(\mathbf{x}_n) \end{bmatrix} \quad (30)$$

Using the Equation 29, the unknown coefficient can be obtained as follow:

$$\{a\} = [R_0]^{-1} \{D\} \quad (31)$$

Substituting the last equation into Equation 27, yields the shape function matrix.

$$u^h(\mathbf{x}) = [R][R_0]^{-1} \{D\} = [N] \{D\} \quad (32)$$

According to the Equation 20, the tangent stiffness matrix changes by increasing the deformation gradient and stresses. Thus, the Equation 19 is a non-linear equation which must be solved using an incremental-iterative procedure. In this paper, the Newton-Raphson method, presented in the next section, is implemented for solving the nonlinear governing equation.

## 6- Newton-Raphson technique

### 6- 1- Incremental load steps

Using the Newton-Raphson technique, the residual force of Equation 19, at the n'th load step can be calculated by the following equation:

$$\{R_n\} = [K_T^n] \{\Delta D_n\} - \{\Delta P_n\} \quad (33)$$

where '[K<sub>T</sub><sup>n</sup>]' is the tangent stiffness matrix at the initial of the load step. The iteration steps should be performed to minimize the residual force.

### 6- 2- Iteration steps

The Newton-Raphson iteration formula is defined as:

$$\{\delta D_n^{k+1}\} = -[K_T^n]^{-1} \{R_n\} \quad (34)$$

Thus, the incremental displacement at the 'k+1'th iteration step can be modified using the following equation.

$$\{\ddot{A}D_n^{k+1}\} = \{\ddot{A}D_n^k\} + \{\delta D_n^{k+1}\} \quad (35)$$

By substituting '{\ddot{A}D<sub>n</sub><sup>k+1</sup>}' into Equation 33 and repeating this process, the residual force vector will be minimized. These iterations will be continued until the size of incremental displacement vector becomes less than a predefined value.

## 7- Numerical results and discussion

### 7- 1- Verification

At the first, a neo-hookean cantilever deep beam subjected to uniform pressure at the free end is considered to verify the accuracy of proposed non-linear meshless method. The dimensions of the beam is considered to be '2\*10' and plane strain condition is supposed (see Figure. 2). The applied traction at the k'th load step is defined as follow:.

$$T_y = f_k = \beta \times k \quad (36)$$

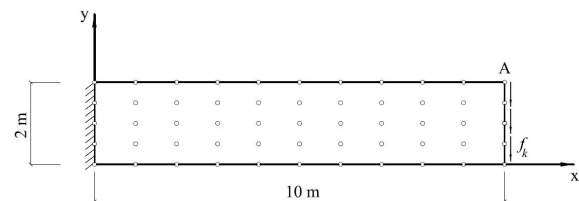


Figure. 2. The sketch of problem

where 'β' is the load scale factor which is selected to be 'β=10'. The loading is applied using ten load incremental steps. The mechanical properties of the beam is selected as [19]:

$$\mu_0 = 0.5 \times 10^4 Pa \quad (37)$$

$$\lambda_0 = 3.3 \times 10^3 Pa \quad (38)$$

The vertical displacement of point 'A' obtained from MLPG method for all load steps are listed in table Table 2 and compared with the reference FEM results. In this table, the percentage difference between the two methods is calculated using the following equation:.

$$e_v(\%) = \left| \frac{v_A^{MLPG} - v_A^{FEM}}{v_A^{FEM}} \right| \times 100 \quad (39)$$

According to this table, the results of proposed method are in good agreement with the FEM.

The load-vertical displacement of point 'A' obtained from linear analysis and geometrically nonlinear analysis for ten load steps is plotted in Figure 3. According to this figure, it can be seen that the deformation of the deep beam is so large that the obtained results from linear and non-linear analysis are significantly different.

**Table 2. The vertical displacement of point ‘A’ compared with the FEM results [19]**

Loading steps		k=1	k=2	k=3	k=4	k=5	k=6	k=7	k=8
FEM [18]	$v_A$	0.816	1.617	2.376	3.078	3.714	4.283	4.768	5.235
MLPG	$v_A$	0.786	1.566	2.318	3.022	3.668	4.251	4.772	5.235
	$e_v$ (%)	3.68	3.15	2.44	1.82	1.24	0.75	0.08	0

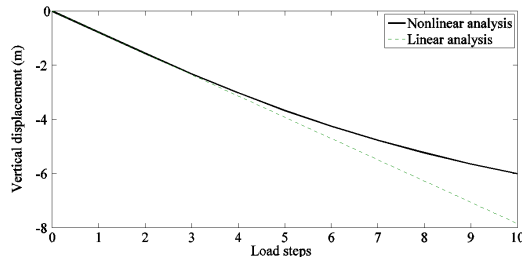


**Figure 3. Comparison between linear and non-linear analyses**

Based on Equation 20, the tangent stiffness matrix in geometrically non-linear problems consists of two parts. The first part is called the ‘linear stiffness matrix’ because it is a function of the geometry and material properties. The second part is called the ‘initial-stress matrix’ and depends on the stress state ‘ $[\bar{S}]$ ’ at the initial of the load steps. The addition of initial-stress matrix, can increase or reduce the stiffness of the structure depend on the stress state. As seen in Figure 3, the neo-hookean cantilever deep beam become stiffer by increasing the load steps.

**7-2- Determination the sufficient number of Monte Carlo simulations**

In this section, the cantilever beam introduced in the previous section is analyzed considering uncertainty in initial elasticity modulus ‘E’. The random values of this property is generated using Monte-Carlo simulation with uniform, normal and lognormal PDFs. The COV of all PDFs is selected to be between 0 to 16 percent. The load scale factor is selected to be ‘ $\beta = 5$ ’ and loading is applied using ten load incremental steps.

The mean value of vertical displacement of point ‘A’ at the end of load steps vs. the number of simulations for normal PDF is plotted in Figure 4. It is obvious from this figure that after ‘600’ simulations convergence has been achieved for various COVs. The variation of mean values of vertical displacement after this number of simulations is less than 1%. The similar diagram is also presented for variance values of vertical displacement in Figure 5. According to this figure, the variance of vertical displacement is converged after ‘400’ simulations so that after this number of simulations, the variation of variance is less than 1%. By increasing the COV, the dispersion of the generated data with various probability density functions increases. Therefore, more simulations are needed to make the mean and variance of results converge to a certain value. According to Figures 4 and 5, one can deduce that for the selected COVs, ‘600’ simulations is sufficient to achieve the results convergence.

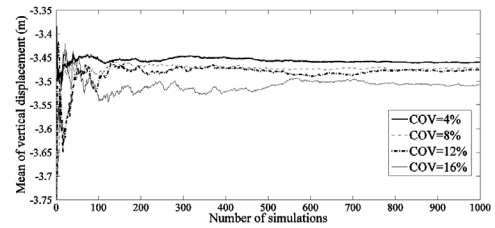


**Figure 4. Determination the sufficient number of simulations for mean convergence of vertical displacement**

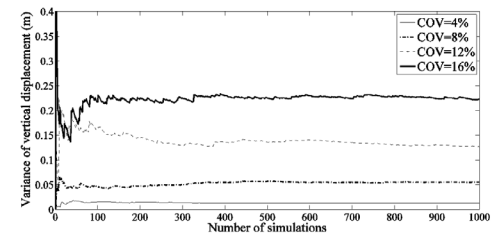


**Figure 5. Determination the sufficient number of simulations for variance convergence of vertical displacement**

**7-3- Stochastic analysis**

In this section, the effects of elasticity modulus PDF and COV on results is studied. For this purpose, the variance of vertical displacement of point ‘A’ at the all load steps for randomly generated elasticity modulus with various COVs in normal distribution is plotted in Figure 6. As can be seen in this figure, the variance of vertical displacement is increased by increasing the COV of initial elasticity modulus. Similar diagram is also plotted for various probability density functions with COV=16%, in Figure 7. According to this figure it can be concluded that the variance of results is also sensitive to elasticity modulus PDF. In addition, according to Figures 6 and 7 it can be seen that at the high load steps, the slope of this diagram is decreased by increasing the load steps. The reason for this matter is that the neo-hookean deep beam becomes stiffer by increasing the load steps.

Figure 8 represents the maximum vertical displacement of point ‘A’ for uncertain elasticity modulus with normal PDF and various COVs in compared with deterministic results at the all load steps. In Table 3, the maximum values of vertical displacement of point ‘A’ at the end of load steps for various PDFs and COVs are listed and compared with the deterministic result. According to this table it can be deduced that maximum vertical displacement in lognormal distribution is more than other PDFs.

**Table 3. Comparison of maximum values of vertical displacement with deterministic result. The vertical displacement obtained from deterministic analysis is equal to '3.570 m'**

PDF	COV (%)	Maximum displacement	Difference percentage
Normal	4	3.852	7.90
	8	4.270	19.61
	12	5.217	46.13
	16	5.686	59.27
Lognormal	4	3.848	7.78
	8	4.287	20.08
	12	4.647	30.17
	16	5.840	63.59
uniform	4	3.747	4.96
	8	4.056	13.11
	12	4.395	23.11
	16	4.833	35.38

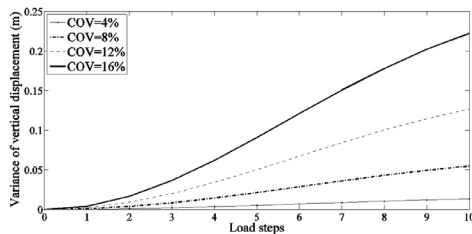


**Figure 6. The variance of vertical displacement of point 'A' at the all load steps for randomly generated elasticity modulus with various COVs in normal PDF**

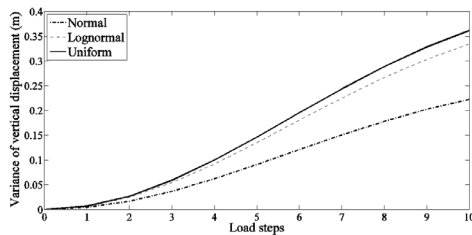


**Figure 7. The variance of vertical displacement of point 'A' at the all load steps for various probability density functions with COV=16%**

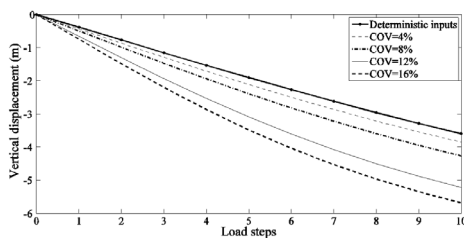


**Figure 8. The maximum vertical displacement for various COVs in normal PDF in compared with the deterministic results**

In Figure 9, the vertical displacement of point 'A' at the end of load steps vs. the sample number for 'COV=16%' in normal distribution is plotted. According to this figure, the minimum and maximum vertical displacements are occurred at the 37<sup>th</sup> (2.32 m) and 327<sup>th</sup> (5.69 m) samples, respectively.

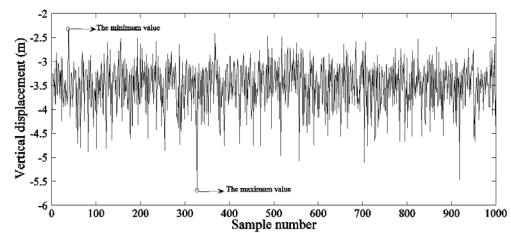


**Figure 9. The vertical displacement of point 'A' at the end of load steps vs. the sample number for 'COV=16%' in normal distribution**

In Figure 10, the maximum, minimum and deterministic values of vertical displacements of point 'A' at the all load steps for 'COV=16%' in normal distribution is presented. According to this figure it can be seen that uncertainty in mechanical properties has significant effect on structural responses.

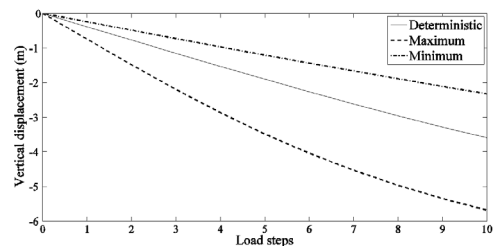


**Figure 10. Maximum, minimum and deterministic results for 'COV=16%' in normal PDF**

#### 7- 4- Result distribution (PDF of results)

The histograms of vertical displacement of point ‘A’ for normal, lognormal and uniform PDFs of elasticity modulus with ‘COV=16%’ are plotted in Figure 11. By comparing these histograms, it can be concluded that the PDF of mechanical properties PDF has a significant effect on results PDF.

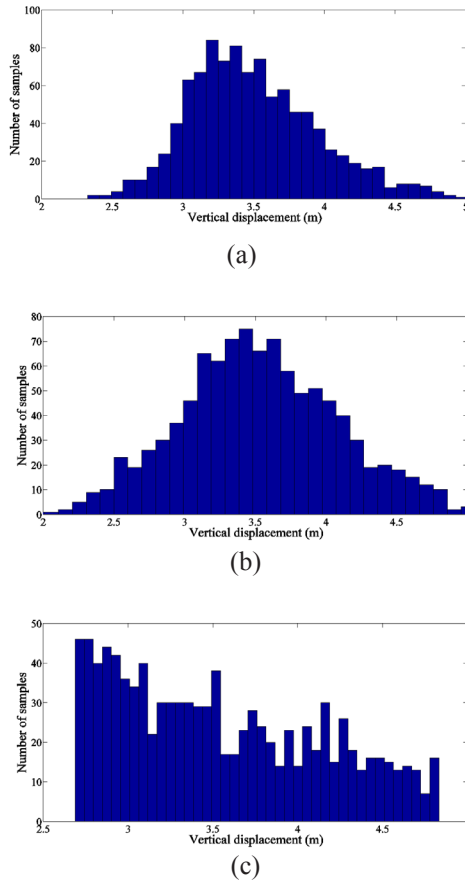


**Figure 11. Histogram of vertical displacement of point ‘A’ for various elasticity modulus PDFs with ‘COV=16%’: (a) normal, (b) lognormal and (c) uniform**

#### 8- Conclusion

In the present study, a neo-hookean cantilever deep beam is studied considering uncertainty in its mechanical properties. A hybrid meshless method which is a composition of MLPG method and Newton-Raphson technique is proposed for geometrically non-linear analysis of structure. The uncertainty of mechanical properties is simulated using MCS technique with normal, lognormal and uniform PDFs and various COVs. Several numerical analyses are carried out to investigate the effects of probability parameters on structural responses. The main results of this paper are outlined as follow:

- The results of deterministic analysis obtained from proposed nonlinear MLPG method match very well with those obtained by FEM.
- The obtained results from linear and nonlinear analysis are significantly different.
- The neo-hookean cantilever deep beam becomes stiffer by increasing the deformations.

- The mean value and variance of vertical displacement vs. the number of simulations at the end of load steps are plotted. It is observed that after 600 simulations, the both parameters are converged.
- For this problem, by increasing the load steps, the variance of results is increased but the slope of diagram at the high load steps is decreased.
- The variance of results is very sensitive to type of elasticity modulus PDF.
- The difference percentage in compared with deterministic results for all PDFs and COV of elasticity modulus are reported in table 3.
- The PDF of mechanical properties has a significant effect on results PDF.

#### References

- [1] S. Chakraborty, B. Bhattacharyya, An efficient 3D stochastic finite element method, *International Journal of Solids and Structures*, 39 (9) (2002) 2465-2475.
- [2] Y. Xu, Y. Qian, G. Song, Stochastic finite element method for free vibration characteristics of random FGM beams, *Applied Mathematical Modelling*, 40 (23) (2016) 10238-10253.
- [3] B.N. Singh, D. Yadav, N.G. Iyengar, AC<sup>o</sup> element for free vibration of composite plates with uncertain material properties, *advanced composite materials*, 11 (4) (2002) 331-350.
- [4] S. Sakata, F. Ashida, K. Ohsumimoto, Stochastic homogenization analysis of a porous material with the perturbation method considering a microscopic geometrical random variation, *International Journal of Mechanical Sciences*, 77 (2013) 145-154.
- [5] S. Naskar, T. Mukhopadhyay, S. Sriramula, S. Adhikari, Stochastic natural frequency analysis of damaged thin-walled laminated composite beams with uncertainty in micromechanical properties, *Composite Structures*, 160 (2017) 312-334.
- [6] A.K. Onkar, C.S. Upadhyay, D. Yadav, Generalized buckling analysis of laminated plates with random material properties using stochastic finite elements, *International journal of mechanical sciences*, 48 (7) (2006) 780-798.
- [7] B.S. de Lima, N.F. Ebecken, A comparison of models for uncertainty analysis by the finite element method, *Finite Elements in Analysis and Design*, 34 (2) (2000) 211-232.
- [8] S.M. Hosseini, F. Shahabian, Reliability of stress field in Al–Al<sub>2</sub>O<sub>3</sub> functionally graded thick hollow cylinder subjected to sudden unloading, considering uncertain mechanical properties, *Materials & Design*, 31 (8) (2010) 3748-3760.
- [9] S.M. Hosseini, F. Shahabian, Stochastic hybrid numerical method for transient analysis of stress field in functionally graded thick hollow cylinders subjected to shock loading, *Journal of Mechanical Science and Technology*, 27 (5) (2013) 1373-1384.
- [10] B.N. Rao, S. Rahman, Stochastic meshless analysis of elastic–plastic cracked structures, *Computational mechanics*, 32 (3) (2003) 199-213.
- [11] S.M. Hosseini, F. Shahabian, J. Sladek, V. Sladek, Stochastic Meshless Local Petrov-Galerkin(MLPG)

- Method for Thermo-Elastic Wave Propagation Analysis in Functionally Graded Thick Hollow Cylinders, *Computer Modeling in Engineering & Sciences (CMES)*, 71 (1) (2011) 39-66.
- [12] M. Dehghan, M. Shirzadi, Meshless simulation of stochastic advection–diffusion equations based on radial basis functions, *Engineering Analysis with Boundary Elements*, 53 (2015) 18-26.
- [13] C. Su, Z. Qin, X. Fan, Stochastic spline fictitious boundary element method for modal analysis of plane elastic problems with random fields, *Engineering Analysis with Boundary Elements*, 66 (2016) 66-76.
- [14] B. Kim, S.B. Lee, J. Lee, S. Cho, H. Park, S. Yeom, S.H. Park, A comparison among Neo-Hookean model, Mooney-Rivlin model, and Ogden model for chloroprene rubber, *International Journal of Precision Engineering and Manufacturing*, 13 (5) (2012) 759-764.
- [15] Y. Anani, G.H. Rahimi, Stress analysis of thick pressure vessel composed of functionally graded incompressible hyperelastic materials, *International journal of mechanical sciences*, 104 (2015) 1-7.
- [16] R.M. Soares, P.B. Gonçalves, Large-amplitude nonlinear vibrations of a Mooney–Rivlin rectangular membrane, *Journal of Sound and Vibration*, 333 (13) (2014) 2920-2935.
- [17] Z.Q. Feng, F. Peyraut, Q.C. He, Finite deformations of Ogden's materials under impact loading, *International Journal of Non-Linear Mechanics*, 41 (4) (2006) 575-585.
- [18] J. Sladek, P. Stanak, Z.D. Han, V. Sladek, S.N. Atluri, Applications of the MLPG method in engineering & sciences: a review, *Comput. Model. Eng. Sci.*, 92 (5) (2013) 423-475.
- [19] Y. Gu, Q.X. Wang, K.Y. Lam, A meshless local Kriging method for large deformation analyses, *Computer Methods in Applied Mechanics and Engineering*, 196 (9-12) (2007) 1673-1684.
- [20] M.H.G. Rad, F. Shahabian, S.M. Hosseini, A meshless local Petrov–Galerkin method for nonlinear dynamic analyses of hyper-elastic FG thick hollow cylinder with Rayleigh damping, *Acta Mechanica*, 226 (5) (2015) 1497-1513.
- [21] M.H.G. Rad, F. Shahabian, S.M. Hosseini, Geometrically nonlinear elastodynamic analysis of hyper-elastic neo-Hookean FG cylinder subjected to shock loading using MLPG method, *Engineering Analysis with Boundary Elements*, 50 (2015) 83-96.
- [22] A.S. Nowak, K.R. Collins, *Reliability of structures*, CRC Press, 2012.
- [23] M.H.G. Rad, F. Shahabian, S.M. Hosseini, Large Deformation Hyper-Elastic Modeling for Nonlinear Dynamic Analysis of Two Dimensional Functionally Graded Domains Using the Meshless Local Petrov-Galerkin (MLPG) Method, *CMES: Computer Modeling in Engineering & Sciences*, 108 (3) (2015) 135-157.
- [24] E. Larsson, B. Fornberg, A numerical study of some radial basis function based solution methods for elliptic PDEs, *Computers & Mathematics with Applications*, 46 (5-6) (2003) 891-902.

Please cite this article using:

M. H. Ghadiri Rad, F. Shahabian, S. M. Hosseini, A geometrically non-linear stochastic analysis of two-dimensional structures made of neo-hookean hyperelastic materials using MLPG method: considering uncertainty in mechanical properties, *AUT J. Civil Eng.*, 2(2) (2018) 209-218.  
DOI: 10.22060/ajce.2018.14531.5483



